FREQUENCY ESTIMATION FOR SENSORLESS CONTROL OF INDUCTION MOTORS

M. Hilairet, F. Auger

GE44, Bd de l'Université, BP406, 44602 Saint-Nazaire cedex, France

{mickael.hilairet,francois.auger}@ge44.univ-nantes.fr

ABSTRACT

In the motor control industry, DSP systems offer major improvements over analog designs, enabling notably to replace speed or position sensors by the implementation of sensorless control algorithms. In this paper, we propose a new viable method which estimates the rotor velocity from the "rotor slot harmonics" included in the stator current signals. This approach is based on both an adjustable digital filter, which is fitted to this particular application, and an extended Kalman filter whose computational burden has been reduced thanks to an additionnal virtual state.

1. INTRODUCTION

Process industries use more and more induction motors instead of DC motors, because of their higher robustness, higher reliability, and lower price [21, 20]. One way to control the speed and torque of these motors is to include tachometers or position transducers in a feedback loop. But these sensors and their wirings are a significant source of failure and cost. When they are mounted on the driving shaft of a single-shaft motor, they are also located at a place which should preferably be assigned to the load. Therefore, their elimination is an attractive prospect, which can be achieved by estimating speed from the stator terminal current measurements (see Fig. 1). This is what is commonly called the sensorless control of induction machines [21].

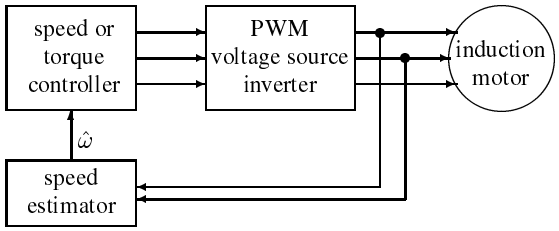

Fig. 1. Block diagram of a sensorless motor drive.

At least three classes of solutions exist to estimate the rotor speed without mechanical sensor. The first one relies on a speed dependent phenomenon called *back emf* [21, 10], which can be described by a dynamic model. This non-linear model can be used to design an adaptive observer, which both estimates the states and the rotor velocity. But this observer is inherently parameter dependent, making the estimation sensitive to parameter uncertainties and to parameter variations caused by internal heating. These parameters may also be tracked [2], but the resulting non-linear model may loose the observability conditions, mainly in steady state and at low speed.

The second kind of solution is based on an active injection of an additionnal carrier-signal voltage [14, 6]. This voltage component produces a carrier-signal current which is modulated by position-dependent leakage inductances. This approach is a promising way, but it may require a modification of the rotor slots, which may also induce torque pulsations. It also requires a voltage source inverter with a high switching frequency.

The third kind of solution, to which our approach belongs, is based on a passive monitoring of the rotor slot harmonics [12, 13]. Mechanical and magnetic saliencies in the rotor (unbalances, eccentricities, variations of the air-gap permeance) generate spectral lines in the current signals whose frequencies and amplitudes do not depend on the motor parameters [8]. This approach is complicated however by the weakness of these harmonics compared to the fundamental frequency, and by the presence of many spectral lines arising both from the voltage source inverter and the motor itself.

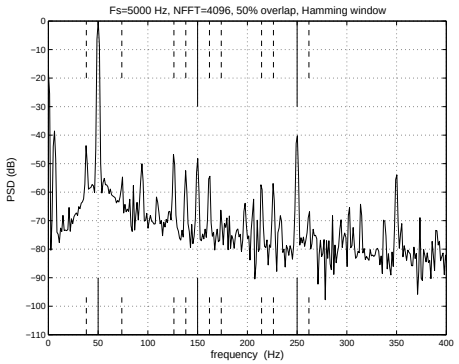

Fig. 2. Estimated power spectral density of the current in one phase of an induction motor in steady-state. The rotor velocity can be recovered from the dashed spectral lines.

To illustrate this, Fig. 2 shows a spectral analysis of the current in one phase of a three-phase 0.7 kW squirrel-cage induction motor operating at 3 Hz (180 rpm) from a sinusoidal (50 Hz) supply (this rather queer operating mode has only been chosen for the readability of the figure). This spectrum includes spectral lines not only at multiples of the fundamental stator frequency (solid lines), but also at frequencies of the form $f_{sh} = n_s\, f_s + n_r\, \frac{N_r}{p}\, f_r$ (dashed lines), where n_s and n_r are two signed integers, and f_s, f_r, N_r and p are respectively the stator frequency, the mechanical rotor frequency, the total number of rotor slots and the number of stator pole pairs. The magnitude of these harmonics can vary with the load [8] and with rotor aging [3].

So as to estimate the rotor frequency f_r from these spectral lines, non parametric (FFT based) approaches can not be used, because of the trade-off between high frequency resolution (obtained with long data records) and quick time response to speed variations (obtained with short data records). Besides, from a statistical point of view, peak picking periodograms yields biased frequency estimates, since the signal includes more than one sinusoid [15]. Other approaches seem to have a large computational burden [12], or to use a very little of the informations available in the current signals [8].

Therefore, we propose in this paper a new approach which tries to comply with most of the practical requirements. This approach, which uses both an efficient adjustable digital filter and a Kalman filter based frequency estimator, is presented in §2. Its good accuracy and fast response are demonstrated in §3. Experimental results are shown in §4.

2. PROPOSED ESTIMATOR

As can be seen on Fig. 2 around 150 Hz, the PSD of the measured currents reveals weak spectral line pairs at frequencies of the form $n_s\, f_s \pm n_r\, \frac{N_r}{p}\, f_r$, where f_s is known *a priori* and f_r is the rotor frequency to be estimated. When sampled with a sampling period T_s, these components become located at the normalized frequencies $\lambda_0 - \delta\lambda$ and $\lambda_0 + \delta\lambda$, with $\lambda_0 = n_s\, f_s\, T_s$ and $\delta\lambda = n_r\, \frac{N_r}{p}\, f_r\, T_s$. Our approach consists in removing everything except these two components thanks to an adjustable two-band filter, and in estimating $\delta\lambda$ (and hence f_r) by a frequency estimator. To this aim, the proposed speed estimation algorithm shown Fig. 3 is made of three building blocks:

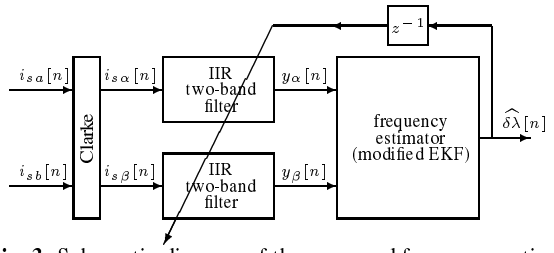

Fig. 3. Schematic diagram of the proposed frequency estimator.

2.1. Clarke transform

This linear transformation builds from the stator currents measured on two phases, i_{s1} and i_{s2}, the coordinates $i_{s\alpha}$ and $i_{s\beta}$ of the stator current in an orthogonal stationary reference frame [21]. Under balanced conditions, the resulting signals are in quadrature. Using these perpendicular signals instead of just one measured current will feed the frequency estimator with more information, and will therefore improve its accuracy and its tracking capability.

2.2. Adjustable two-band filters

The two signals $i_{s\alpha}$ and $i_{s\beta}$ are then filtered by two identical IIR multi-band filters, which have two pass-bands centered on $\lambda_0 - \delta\lambda$ and $\lambda_0 + \delta\lambda$, so as to enhance the two information-bearing signal components, and to remove as much as possible the irrelevant stator harmonic λ_0 and the neighbouring rotor slot harmonics $\lambda_0 \pm 2\delta\lambda$. So as to track varying frequencies, the coefficients of these filters must be deduced from the design parameters λ_0 and $\delta\lambda$ by analytic expressions. Several approaches can be used to design such adjustable filters. We used a simple scheme using two second order all-pass sections [18], shown Fig. 4. The resulting transfer function is

$$\mathcal{H}_{2b}(z) = 1 - \frac{1}{2}\left(\mathcal{H}_{lsb}(z) + \mathcal{H}_{usb}(z)\right), \quad (1)$$

$$\text{with } \mathcal{H}_{lsb}(z) = \frac{r^2 - (1+r^2)\,\beta_{lsb} z^{-1} + z^{-2}}{1 - (1+r^2)\,\beta_{lsb} z^{-1} + r^2 z^{-2}}, \quad (2)$$

$$\mathcal{H}_{usb}(z) = \frac{r^2 - (1+r^2)\,\beta_{usb} z^{-1} + z^{-2}}{1 - (1+r^2)\,\beta_{usb} z^{-1} + r^2 z^{-2}}, \quad (3)$$

$$\beta_{lsb} = \cos(2\pi(\lambda_0 - \delta\lambda),$$

$$\beta_{usb} = \cos(2\pi(\lambda_0 + \delta\lambda),$$

$$r^2 = \frac{1 - \tan(\pi\Delta\lambda)}{1 + \tan(\pi\Delta\lambda)}$$

When $\frac{\delta\lambda}{\Delta\lambda} \gg 1$, $\Delta\lambda$ is the bandwidth in both frequency bands. The main justifications of our choice are an appropriate behaviour at low speed (when $\delta\lambda \approx 0$, $\mathcal{H}_{2b}(z)$ is a band-pass filter centered on λ_0), and the existence of an efficient implementation whose robustness against truncation errors allows its use on fixed point processors [18].

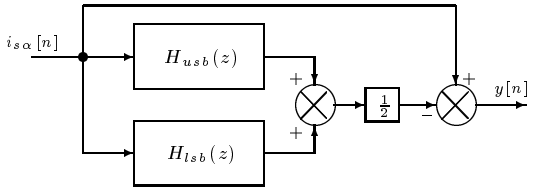

Fig. 4. Block diagram of the adjustable two-band filter.

2.3. Frequency estimator

Extended Kalman filters (EKF) [1, 9] are privileged tools to estimate the amplitude, phase and frequency of a single sinusoid [16, 5] or of multiple sinusoids [17] from noisy measurements. Their design proceeds from a linear state space model of the signal, the frequencies being considered as known *a priori*. The state space model is then extended to the vector Θ of the unknown frequencies, which are supposed to be slowly varying, and the model describing the evolution of this extended state becomes nonlinear. The conventional equations of these filters are summarized in Table 1.

In our case, if the state is made of four in-phase and quadrature signals (as in [16]) and the unknown (angular) frequency parameter $\theta = 2\pi\,\delta\lambda$, the computational cost of a conventional extended Kalman filter will be large, requiring one matrix inversion and several matrix sums and products. However, it should be pointed out that the transition matrix A_d and the observation vector C of the linear model both include 2×2 submatrices with equal terms on the diagonal and opposite terms on the anti-diagonal.

$$A_d[k] = \begin{bmatrix} a_{11} & b_{11} & 0 & 0 \\ -b_{11} & a_{11} & 0 & 0 \\ 0 & 0 & a_{22} & b_{22} \\ 0 & 0 & -b_{22} & a_{22} \end{bmatrix}, \quad (4)$$

$$C = \begin{bmatrix} 1 & 0 & 1 & 0 \\ 0 & 1 & 0 & 1 \end{bmatrix}, \quad (5)$$

$$\text{with } a_{11} = \beta_{usb}, \quad b_{11} = -\sin(2\pi(\lambda_0 + \delta\lambda)), \quad (6)$$

$$a_{22} = \beta_{lsb}, \quad b_{22} = -\sin(2\pi(\lambda_0 - \delta\lambda)) \quad (7)$$

State and parameters prediction

$$\begin{aligned} X[k+1|k] &= A_d[k]\, X[k|k] \\ \Theta[k+1|k] &= \Theta[k|k] \end{aligned}$$

A priori covariance matrix computation

$$\begin{aligned} P[k+1|k] &= F[k]\, P[k|k]\, F[k]^t + Q \\ F[k] &= \begin{bmatrix} A_d[k] & \frac{\partial}{\partial\Theta}(A_d[k]\, X[k|k])_{\Theta[k|k]} \\ 0 & I \end{bmatrix} \end{aligned}$$

Kalman gain computation

$$\begin{aligned} K[k+1] &= P[k+1|k]\, H^t (H\, P[k+1|k]\, H^t + R)^{-1} \\ H &= [\ C \quad 0\ ] \end{aligned}$$

State and parameters correction

$$\begin{bmatrix} X[k+1|k+1] \\ \Theta[k+1|k+1] \end{bmatrix} = \begin{bmatrix} X[k+1|k] \\ \Theta[k+1|k] \end{bmatrix} + K[k+1]\,(Y[k+1] - C\, X[k+1|k])$$

A posteriori covariance matrix computation

$$P[k+1|k+1] = P[k+1|k] - K[k+1]\, H\, P[k+1|k]$$

Table 1. Conventional extended Kalman filter equations

So as to force the F matrix to also satisfy this structural property, we propose to include in the parameter vector Θ a *virtual* parameter θ_v ($\Theta = (\theta\ \theta_v)^t$). This new parameter is supposed to be nearly constant ($\theta_v[k+1] = \theta_v[k] + v_6[k]$, where $v_6[k]$ is a zero-mean noise process) and to be *virtually* bound to the signal model so that

$$F[k] = \begin{bmatrix} & & & & f_1 & -f_2 \\ & A_d[k] & & & f_2 & f_1 \\ & & & & f_3 & -f_4 \\ & & & & f_4 & f_3 \\ 0 & 0 & 0 & 0 & 1 & 0 \\ 0 & 0 & 0 & 0 & 0 & 1 \end{bmatrix} \quad (8)$$

$$(f_1\ f_2\ f_3\ f_4)^t = \frac{\partial}{\partial\theta}(A_d[k]\, X[k|k])_{\theta[k|k]} \quad (9)$$

$$f_1 = b_{11}\, x_{r\alpha} - a_{11}\, x_{r\beta} \quad (10)$$

$$f_2 = a_{11}\, x_{r\alpha} + b_{11}\, x_{r\beta} \quad (11)$$

$$f_3 = -b_{22}\, x_{l\alpha} + a_{22}\, x_{l\beta} \quad (12)$$

$$f_4 = -a_{22}\, x_{l\alpha} - b_{22}\, x_{l\beta} \quad (13)$$

The main theoretical innovation brought by this paper is that if Q and R are chosen so as to also satisfy this structural property, then the two covariance matrices $P[k+1|k]$ and $P[k+1|k+1]$ and the correction gain $K[k+1]$ have the following structure:

$$P = \begin{bmatrix} P_{11} & 0 & P_{13} & P_{14} & P_{15} & P_{16} \\ 0 & P_{11} & -P_{14} & P_{13} & -P_{16} & P_{15} \\ P_{13} & -P_{14} & P_{33} & 0 & P_{35} & P_{36} \\ P_{14} & P_{13} & 0 & P_{33} & -P_{36} & P_{35} \\ P_{15} & -P_{16} & P_{35} & -P_{36} & P_{55} & 0 \\ P_{16} & P_{15} & P_{36} & P_{35} & 0 & P_{55} \end{bmatrix} \quad (14)$$

$$K^t = \begin{bmatrix} K_{11} & -K_{14} & K_{13} & K_{14} & K_{15} & K_{16} \\ K_{14} & K_{11} & -K_{14} & K_{13} & -K_{16} & K_{15} \end{bmatrix} \quad (15)$$

This result reduces the number of distinct values in these matrices, and allows the extended Kalman filter to be implemented by *scalar* recurrence equations. This also forces the estimation errors on the in-phase and quadrature components to be uncorrelated, since $P_{12} = P_{34} = P_{56} = 0$. Since the Kalman gain is not changed when both Q and R are multiplied by the same scalar, and since there is no reason to consider differently the two signal components, we chose $Q = \mathrm{diag}\,(q_1, q_1, q_1, q_1, q_3, q_3)$ and $R = \boldsymbol{I}_2$. So as to comply with the four-page limit of these proceedings, the complete equations of the Kalman filter are not presented here, but can be found in an internal report available on the web [11], where supplementary informations can also be found.

Finally, so as to track time-varying frequencies, the frequency deflection $\widehat{\delta\lambda}$ estimated by the EKF is used at the next time sample to update the two-band filter coefficients.

Table 2 shows the number of arithmetic operations required at each time sample by our algorithm, compared to a straightforward matrix-based implementation of a 5-state extended Kalman filter, as the one obtained with an automatic C code generator. The complexity and the memory requirements are significantly lowered by the use of an additionnal virtual state, as already shown in [10] for another application. For the evaluation of the total number of arithmetic operations, the trigonometric functions required by the estimator are supposed to be computed by fifth degree polynomials, as done for example on DSP's [19]. The three trigonometric functions are therefore equivalent to 15 multiplications and 15 additions.

Computation of	number of multiplications and inversions		Number of additions	
two-band filters	22		30	
A_d	24	(40)	24	(48)
F	0	(8)	0	(4)
$X[k+1\|k]$	8	(16)	4	(12)
$P[k+1\|k]$	45	(250)	33	(225)
$K[k+1]$	7	(146)	7	(111)
$P[k+1\|k+1]$	16	(165)	22	(145)
$\begin{bmatrix} X[k+1\|k+1] \\ \Theta[k+1\|k+1] \end{bmatrix}$	10	(20)	14	(20)
Total	109	(645)	104	(566)

Table 2. Number of operations by iteration for the two-band filters and for an efficient (or a rough) implementation of the extended Kalman filter.

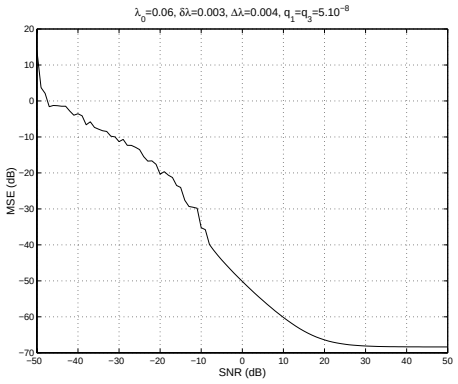

Fig. 5. Mean square error versus signal noise ratio in steady state.

3. STATISTICAL AND TRACKING PROPERTIES

Since the proposed estimator is highly nonlinear, numerical simulations are an important part of evaluating its performance. We first examined the estimation accuracy in steady state. Fig. 5 shows the mean square error versus the signal noise ratio (both in decibels) of the EKF output $\widehat{\delta\lambda}$ computed during 5 seconds (with sampling frequency $F_s = 2500$ Hz) over 50 independant Monte Carlo experiments. The signal is made of 5 equal amplitude components at

frequencies λ_0, $\lambda_0 \pm \delta\lambda$ and $\lambda_0 \pm 2\delta\lambda$. The threshold of satisfactory performance is around -10 dB, which is completely in accordance with the industrial context. Computer simulations were also performed to evaluate the tracking behaviour of the proposed algorithm. After an initialisation of the algorithm in steady state, we performed either abrupt changes or linear variations of frequency. The signal has the same structure as in Fig. 5, and the SNR is 0 dB. The central frequencies of the two-band filters are frozen (open loop estimator) during the first 250 points. Fig 6 shows some of the obtained results. Future works will try to compare these results with some previous approaches.

4. EXPERIMENTAL RESULTS

An experimental validation of the proposed algorithm was carried out on a 0.7 kW squirrel cage induction motor connected to an inertial load. Fig. 7.a shows the speed estimation error obtained with the signals already used for Fig. 2, and with a speed initialization 9 rpm above the real value. A correct estimation is reached after nearly 1 s ($F_s = 2500$ Hz). Fig 7.b shows a linear speed variation from 1000 to 800 rpm, which confirms the tracking capability of the algorithm in a real situation.

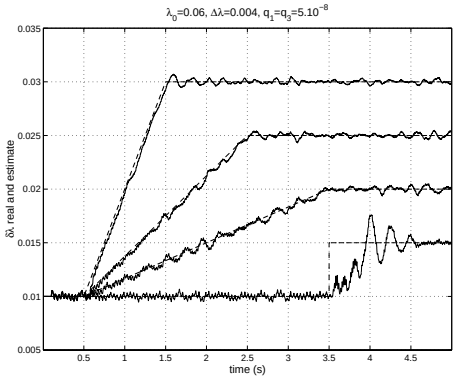

Fig. 6. Tracking capability of the proposed algorithm evaluated on one abrupt change and 3 linearly increasing frequencies, equivalent to a speed variation from 375 rpm to 562.5, 750, 937.5 and 1125 rpm respectively.

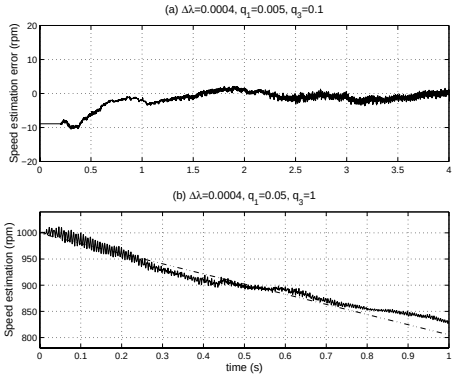

Fig. 7. Experimental results obtained during a steady state (a) and a speed variation (b).

5. REFERENCES

[1] B.D.O. Anderson, J.B. Moore, Optimal filtering, Prentice Hall, 1979.

[2] D. Atkinson, P. Acarnley, J. Finch, " Observers for induction motor state and parameter estimation," *IEEE Trans on Ind Applicat*, Vol 27, No 6, pp 1119–1127, Nov 1991.

[3] M. E-H Benbouzid, M. Vieira, C. Theys, "Induction motors faults detection and localization using stator current advanced signal processing techniques," *IEEE Trans on Power Electron*, Vol 14, No 1, pp 14–22, jan 1999.

[4] R. Blasco-Giménez, "Comments on "sensorless speed measurement using current harmonic spectral estimation in induction machines drives"," *IEEE Trans on Power Electron*, Vol 12, No 5, pp 938-940, 1997.

[5] P.K. Dash *et al*, "An extended complex Kalman filter for frequency measurement of distorted signals," *IEEE Trans on Istrum. Meas.*, Vol 49, No 4, pp 746–753, aug 2000.

[6] M.W. Degner, R.D. Lorenz, "Position estimation in induction machines utilizing rotor bar slot harmonics and carrier-frequency signal injection," *IEEE Trans on Ind Applicat*, Vol 36, No 3, pp 736–742 , may 2000.

[7] T. Du, "Joint state and parameter estimation of induction motor drives with application to adaptative Field Oriented Control," PhD Thesis, University of Birmingham, 1993.

[8] A. Ferrah *et al*, "A speed identifier for induction motor drives using real-time adaptive digital filtering," *IEEE Trans on Ind Applicat*, Vol 34, No 1, pp 156–162, jan 1998.

[9] M.S. Grewal, A.P. Andrews, "Kalman filtering, theory and practice," Prentice Hall, 1995.

[10] M. Hilairet, F. Auger, C. Darengosse, "Two efficient Kalman filters for flux and velocity estimation of induction motors," *Proc IEEE PESC'00*, Vol 2, pp 891–896, june 2000.

[11] M. Hilairet, F. Auger, "Sensorless speed measurement," internal report, `http://crttsn.univ-nantes.fr/~auger/publis/icassp2001`.

[12] K.D. Hurst, T.G. Habetler, "Sensorless speed measurement using current harmonic spectral estimation in induction machine drives," *IEEE Trans on Power Electron*, Vol 11, No 1, pp 66–73, jan 1996.

[13] K.D. Hurst *et al*, "A self tuning closed-loop flux observer for sensorless control of induction machines," *IEEE Trans on Power Electron*, Vol 12, No 5, pp 807–815, sept 1997.

[14] P.L. Jansen, R.D. Lorenz, "Transducerless position and velocity estimation in induction AC machines," *IEEE Trans on Ind Applicat*, Vol 31, No 2, pp 240–247, march 1995.

[15] S. Kay, "Modern spectral estimation," Prentice Hall, 1998.

[16] B.F. La Scala, R.R. Bitmead, "Design of an extended Kalman filter frequency tracker," *IEEE Trans Signal Processing*, Vol 44, No 3, pp 739–742, march 1996.

[17] P.J. Parker, B.D.O. Anderson, "Frequency tracking of non-sinusoidal periodic signals in noise," *Signal Processing*, Vol 20, No 2, pp 127–152, june 1990.

[18] P.A. Regalia, S.K. Mitra, P.P. Vaidyanathan, "The digital all-pass filter : A versatile signal processing building block," *Proc IEEE*, Vol 76, No 1, pp 19-37, 1988.

[19] G. Sitton, "A collection of functions for the TMS320C30," *Texas Instruments application report SPRA 117*, 1997.

[20] Texas Instruments Inc., *"Digital signal processing solution for AC induction motor,"* Application note BPRA043, 1996.

[21] P. Vas, "Sensorless vector and direct torque control," *Oxford University Press*, 1998.